Soft Matter

Accepted Manuscript

ROYAL SOCIETY OF CHEMISTRY

www.rsc.org/softmatter

Graphic for the Table of Contents

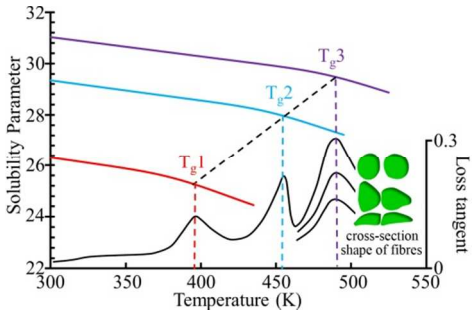

Soft Matter

RSCPublishing

ARTICLE

Understanding the Variability of Properties in *Antheraea Pernyi* Silk Fibres

Cite this: DOI: 10.1039/x0xx00000x

Yu Wang,[a] Juan Guan,[b, c] Nick Hawkins,[b] David Porter*[b] and Zhengzhong Shao*[a]

Received 00th January 2012,
Accepted 00th January 2012

DOI: 10.1039/x0xx00000x

www.rsc.org/

Variability is a common feature of natural silk fibres, caused by a range of natural processing conditions. Better understanding of variability will not only be favourable for explaining the enviable mechanical properties of animal silks but will provide valuable information for the design of advanced artificial and biomimetic silk-like materials. In this work, we have investigated the origin of variability in forcibly reeled *Antheraea pernyi* silks from different individuals using dynamic mechanical thermal analysis (DMTA) combined with the effect of polar solvent penetration. Quasi-static tensile curves in different media have been tested to show the considerable variability of tensile properties between samples from different silkworms. The DMTA profiles (as a function of temperature or humidity) through the glass transition region of different silks as well as dynamic mechanical properties after high temperature and water annealing are analysed in detail to identify the origin of silk variability in terms of molecular structures and interactions, which indicate that different hydrogen bonded structures exist in the amorphous regions and they are notably different for silks from different individuals. Solubility parameter effects of solvents are quantitatively correlated with the different glass transitions values. Furthermore, the overall ordered fraction is shown to be a key parameter to quantify the variability in the different silk fibres, which is consistent with DMTA and FTIR observations.

Introduction

Animal silks are natural protein fibres spun by a wide range of insects and spiders,[1] which have aroused great scientific interest due to their excellent mechanical properties of combined toughness and strength that are unattainable by most man-made and biomimetic fibres.[2-9] Therefore, many attempts have been made to relate these mechanical properties to the hierarchical structural features of silks in terms of quantitative structure-property relations.[10-21] While understanding differences between different silk types has been an important part of silk research, the issue of variability between silk from different individuals within a species or even the same individual is an important feature, [22-28] both commercially in terms of textile silk 'quality' and also scientifically to look into the interactions between processing, structure and silk properties.[14, 29, 30] Detailed studies of spider silks and *Bombyx mori* (*B. mori*) silkworm fibres have identified variability in both extrinsic properties such as fibre diameter and shape, and intrinsic properties such as stress-strain relations of modulus and failure stress.[23, 26, 27, 30-33] Although extrinsic properties are clearly important for the performance of silk fibres, understanding the structural factors that cause variability in intrinsic properties is the focus of this work, since this will be important to guide the development of high performance synthetic and bio-inspired polymeric materials.

Dynamic mechanical thermal analysis (DMTA) has become an important analytical technique for exploring the structure-property relationships of amorphous or semicrystalline synthetic polymers.[34] So far, only a limited number of studies have been carried out to investigate the thermomechanical properties of various silk fibroins (natural silk fibres, regenerated silk fibroin (RSF) fibres and films and silk composites) using DMTA, and some have focused on silk structure-property relationships.[35-42] Previously, for example, Yang, *et al*.[37] studied the counterintuitive toughness of spider silk at low temperature and correlated it to loss peak at -70 ^{o}C. Applying uniaxial tension to different post-draw ratio films, Yin *et al*.[39] prepared RSF films with enhanced toughness in the dry state, and the mechanism of drawing-induced separation of amide-amide and side chain interactions was proposed, based on the DMA evidence.

Recently, Guan *et al*.[42-44] systematically investigated the link between structure and dynamic mechanical properties of silks. Specifically, they studied the dynamic mechanical properties of *B. mori* and spider dragline silks as a function of load, humidity, temperature and thermal history using DMTA. Their results indicated that property changes below 100 °C are due mainly to evaporation of water with increasing temperature and the various discrete loss tangent peaks above 100 °C are due to specific disordered structures in silk fibres. These higher temperature loss peaks were then used to characterize the effects of different processing conditions on *B. mori* silks, such as force reeling and RSF fibres on mechanical properties.[45] These studies provide valuable background and open a "window" for using DMTA on silk fibres from other species or types.

Antheraea pernyi (*A. pernyi*) silk is a kind of wild silkworm silk that is used to construct a cocoon, like the domesticated commercial *B. mori* silk, but has a similar amino acid sequence to some spider (major ampullate) silks.[46, 47] Generally, both types of silk contain repetitive regions composed of alternating polyalanine region and glycine-rich regions, although the repetitive alanine sequences (poly(Ala)$_{12\text{-}13}$) in *A. pernyi* silk are longer than that in most spider major ampullate silks (poly(Ala)$_{6\text{-}9}$). In this respect, it is interesting

to study the structure-property relationships of this species as a sort of generic example of the whole animal silk family. However, earliest studies on *A. pernyi* silk fibroin mainly concentrated on structural analysis of conformation transition of films cast from either native[48, 49] or regenerated[50-52] silk fibroin solution, which show that α-helix is the major conformation in these films, which can be converted to β-sheet structure by thermal or methanol treatment.

Systematic studies have been conducted on natural *A. pernyi* silks, with the aim of understanding the relationship between structure and properties.[18, 53, 54] Fu *et al*.[18] compared the mechanical properties of forcibly reeled *A. pernyi* silks with those of spider major ampullate silks and *B. mori* silks and proposed a model correlating the mechanical properties of the silks to their intrinsic ordered fraction, which suggests that these three kinds of silks share comparable structure-property relations, as proposed by Porter.[15] Later, Ling *et al.*[53] investigated the content of secondary structures (β-sheet, α-helix and random coil) and their orientation in single *A. pernyi* silks as well as the change in both aspects with tensile deformation using synchrotron FTIR microspectroscopy. Although these studies are of great value for a general understanding this kind of silk, the specific structural features that control the variability in the detailed mechanical properties of *A. pernyi* silk remain unknown.

More recently, we investigated the effect of polar solvents with different molecular sizes on the structure and tensile properties of forcibly reeled *A. pernyi* silks and found that silks from different individuals show significantly different response to the same solvent, and even in air without solvent.[54] We proposed that the varying free volumes in the amorphous regions should be the main structural origin of variability in as-reeled *A. pernyi* silks from different individuals. However, we left open the question about the molecular origin of this structural variability, which is the main subject of the present study. To this end, for the first time, we investigated the origin of variability in as-reeled *A. pernyi* silks by a combination of DMTA and solvent penetration. After measuring the variability of conventional stress-strain properties of different as-reeled *A. pernyi* silks in different media, we then studied the dynamic mechanical properties of different samples as a function of temperature, humidity and time, and compared the results after high temperature and water annealing. Finally, the relations between solubility parameter effects and glass transitions were quantitatively analysed. These observations allow us to suggest a relatively simple and self-consistent origin for variability that should add to the overall understanding of silk structure and properties.

Experimental section

Silk Fibre Preparation

Silk fibres used here were all forcibly reeled at 8 mm/s[3, 24] in Lab conditions (20 °C, 40% RH) from mature *A. pernyi* silkworms, which previously lived on oak trees in a tussah field of Shandong province, China. Forcibly reeling silks from the spinneret of mature *A. pernyi* silkworm is more convenient and controllable than the same procedure applied on *B. mori* silkworms,[30] which generates nearly defect-free silks. The silks were collected and restrained on a plastic cylinder of 21mm in diameter and then stored under Lab conditions before being tested. The silks from the same silkworm were collected in the same spinning session on the same day, and were found to have consistent cross-sections. Segments of silk fibres (bave) with a gauge length of 5 ± 0.1 mm were then transferred and adhered onto the sample-holders[42] made from hard cardboard (for testing in air) or aluminum foil (for testing in solvents) with cyanoacrylate. For the measurements, the side support of the frame was simply cut away, so that the force was transmitted through the silk fibre.

Cross-sectional Area Measurement

The cross-sectional area of the as-reeled silk fibre was measured according to the method described in detail elsewhere.[30] Briefly, the silk fibres were glued (along their length) as straight as possible onto a section of solder wire with cyanoacrylate and dried for 2~3 h, then another layer of glue was brushed onto its surface. After drying overnight, the solder wire was sectioned directly using fresh razor blades. The thin discs were then treated with 200 μL mL^{-1} protease solution in a 38 °C incubator for about 24 h. These discs were then mounted onto a SEM stub and sputtered under 18 mA for 150 s, giving a 12.5 nm coating of gold/palladium (Quorum Technologies SC7620). The cross sections were observed by a Jeol Neoscope JCM-5000 with secondary electrons at 10 kV and x2200 magnification. Digestion treatment of silk fibre gives an outline in the glue equal to the silk's original cross section. From this outline, we estimated the cross sectional area of the silk fibre using ImageJ software (NIH). Usually, 8 to 10 well-defined cross sectional images should be obtained from a silk fibre for area measurement. The average area was used as the cross sectional area of adjacent as-reeled silk fibres. The area of the contracted silk fibre was calculated with the tested hypothesis that its volume was constant after contraction. We take no account of the influence of sericin coating on the cross sectional area as well as the properties discussed below, because the sericin coating on the fibre's surface is uniform along the silk fibre and extremely thin (100-200 nm in thickness) compared to the greater thickness of a single brin of *A. pernyi* silk (15-17 μm) (See Figure S1, for example).

Tensile Testing

Quasi-static tensile tests in air were performed on TA Q800 in controlled-force mode, around 20 °C at a force-ramp rate of 0.1 N/min. Before the tests in air, a 15−20 min dry nitrogen purge was applied to remove the excess moisture. The measurements in selected solvents (water, methanol, and ethanol) were carried out using submersion clamp after immersion for 15 min and no load was exerted on the fibre during the pre-test immersion time, in order to allow for any possible contraction of the fibre. The solvents were sucked off from the top of the liquid cell after the test finished.

Dynamic Mechanical Thermal Analysis

All the DMTA tests were performed on a TA Q800 under DMA multi-frequency strain mode. The dynamic mechanical test through a temperature range is called "temperature scan". The isothermal dynamic mechanical test at room temperature through a time range is regarded as "isothermal time scan". The constant parameters for all the DMTA tests are as follows: (i) the frequency at 1Hz, (ii) the dynamic strain at 0.1%, (iii) the preload force equivalent to 30 MPa (except time scan) stress was applied to keep the test fibre in tension to make sure of the dynamic oscillation not falling out of tension.

A temperature ramp rate of 3 °C /min was used for all the temperature scan tests and two DMTA procedures were developed: (1) full range temperature scan from -100 °C to +300 °C; (2) cyclical temperature scans with the first ramp up to +175 °C and called +175 °C annealing.

For the humidity dynamic tests, a humidity accessory was adapted to control the humidity scan with constant temperature. The resolution of temperature was 1 °C, and the relative humidity was 2%. The set-up parameters for the humidity dynamic test are as follows: humidity ramps from 0% to about 90% at setting temperature (80 °C) at 1%/min after 30 min of equilibrium after the target temperature was reached.

The isothermal time scan was performed in different media at room temperature ~20 °C under various static stresses: 50 MPa, 100 MPa, 150 MPa, 200 MPa and 300 MPa. Before the test, a 15−20 min dry nitrogen purge was applied to remove the excess moisture. To improve the accuracy and consistency of the results, an individual fibre was used for the time scan in all media. One solvent was extracted after the dynamic mechanical properties of the sample reach equilibrium in this solvent. The solvent added to the liquid cell follows the sequence of ethanol, methanol, and water.

Results and discussion

Variability of tensile performance in different media

In our previous work, silk fibres from 10 different silkworms were grouped into four generic types of samples mainly according to their different tensile behaviour in methanol and ethanol.[54] Here, silk fibres from three individual silkworms (labelled arbitrarily as silkworms 1, 2 and 3), which represent the limits and mid-point of the distribution of properties, were chosen to investigate the origin of variability in as-reeled *A. pernyi* silks. In the beginning, we compared their tensile performance in different media to demonstrate their obvious variability of properties. As shown in Figure 1a, the stress-strain curves of as-reeled *A. pernyi* silks from the same individual are fairly consistent in the dry state, while the stress-strain curves of as-reeled *A. pernyi* silks from different individuals show noticeable variability. More specifically, the silk fibres from silkworm 3 display higher modulus, yield stress and tenacity, but lower extensibility and toughness than those from silkworm 1, and the silk fibres from silkworm 2 show intermediate values (Table 1).

Table 1 Mechanical properties of as-reeled *A. pernyi* silks

Samples	Initial elastic modulus (GPa)	Post-yield modulus (GPa)	Yield stress (MPa)	Breaking strain (%)	Breaking stress (MPa)	Breaking energy ($MJ \cdot m^{-3}$)
Silkworm 1(n=6)	8.6 ± 0.5	0.51 ± 0.05	241 ± 3	75 ± 7	525 ± 27	259 ± 25
Silkworm 2(n=6)	9.9 ± 0.5	0.75 ± 0.07	268 ± 11	40 ± 4	549 ± 33	154 ± 20
Silkworm 3(n=5)	11.8 ± 0.4	1.52 ± 0.09	318 ± 27	23 ± 2	628 ± 29	106 ± 9

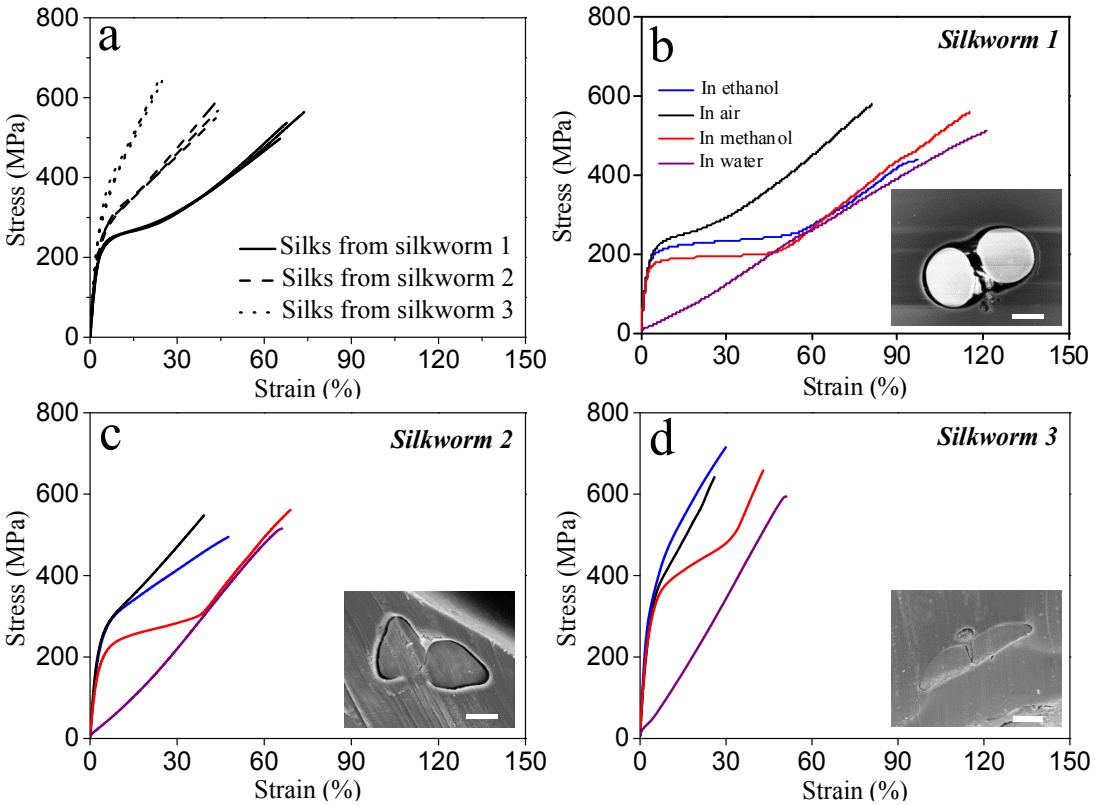

Figure 1. Typical stress-strain curves of as-reeled *A. pernyi* silks from different individuals (a) tested in dry air using DMTA at quasi-static rates. Typical stress−strain curves submerged in ethanol and methanol as well as control samples in dry air and water: as-reeled *A. pernyi* silks from silkworms 1 (b), 2 (c) and 3 (d). Inserts are the cross sections of silk-embedded cyanoacrylate after digested in a protease solution. The scale bars represent 10 μm. Legend is the same for (b), (c), and (d).

The stress-strain curves for the three silks in different solvents are shown in Figure 1b to 1d. In water, all are almost straight lines from the origin, with a modulus equal to the post-yield dry modulus tested in air. On exposure to methanol, all the stress-strain curves follow the tensile curves of the dry state in the initial linear elastic region. But after yield, both the stress-strain curves of samples from silkworm 1 (Figure 1b) and 2 (Figure 1c) move across to the same curves as the wet state, while the stress-strain curve of the silk fibre from silkworm 3 (Figure 1d) only partially shifts towards the curve in water and then runs parallel at higher stress. However, for immersion in ethanol, the tensile curves of silk fibres from these 3 silkworms differ remarkably from one another: Samples from silkworm 1 (Figure 1b) behave in a similar way to those with methanol; samples from silkworm 2 just diverge from the stress−strain curves in dry air at higher stress after yield (Figure 1c); and sample 3 follows that of dry air, with a slightly higher post-yield modulus (Figure 1d). Undoubtedly, these properties derive from the intrinsic structural variability in the silk fibres, which is described and analysed in the following section. Nevertheless, we must also note that these three silkworms have a different response to the reeling process, as confirmed by the shapes of the three cross sections (inserts of Figure 1b-d) of the silk fibres from the different silkworms,[18] and this must be an extrinsic origin for the variability of silks from different individuals, which cannot be explored here.

DMTA on as-reeled *A. pernyi* silks from different individuals

Typical DMTA plots of as-reeled *A. pernyi* silk with the changes of two dynamic mechanical properties (storage modulus and loss tangent) and static length as a function of changes in temperature are shown in Figure 2a. The curves follow the general rules that decreases in storage modulus with temperature are associated with peaks of loss tangent (more energy dissipated means less energy stored) and any increases in storage modulus should be due to a reconfiguration of the polymer into a stronger bonded structure, usually following a dynamic relaxation step.[15,42]

Generally, the storage modulus decreases at first with the increase of temperature from -100 °C and the loss tangent curve displays two broad loss peaks at about -65 °C and 60 °C, which have been assigned to property changes associated with water for *B. mori* silks and spider dragline silks.[42] When the temperature reaches about +110 °C, the storage modulus begins to drop more rapidly, accompanied by a loss tangent peak at around +128 °C. Rather unexpectedly, the modulus rises suddenly when the temperature goes above +180 °C and the corresponding sharp loss tangent peak appears at around +182 °C. Eventually, the storage modulus drops significantly again until the temperature falls to +270 °C, accompanied by the largest loss tangent peak at +220 °C and a prominent increase of static length under constant static stress associated with the drop in storage modulus. The dynamic mechanical properties of silks at higher temperature (T > 100 °C) associated with the glass transitions of silk fibroin is the main focus of our exploration here, since it provides most information about structure-property relations of as-reeled *A. pernyi* silks. The position and height of three characteristic loss tangent peaks through the glass transition range are the main measures of structural diversity, because different hydrogen bonded structures in the amorphous region should be associated with different T_g peaks.[40, 42]

Based on this premise, Figure 2b compares the temperature scans of the silk fibres from different individuals studied here. All three silks show two lower temperature loss peaks between 120 °C and 185 °C, which should be associated with more 'disordered' structures, i.e., amorphous structures with less intermolecular hydrogen bonding.[15, 42] However, these two glass transition events are significantly different for silks from different individuals, which reflect different hydrogen bonded structures in the more disordered regions. After examining the storage modulus-temperature curves (Figure S2a), we found that all three samples show the abrupt rise of modulus in the temperature range from 165 °C to 185 °C, which may arise from a structure relaxation through this specific glass transition that stiffens all the silk fibres, which is discussed further below as annealing.

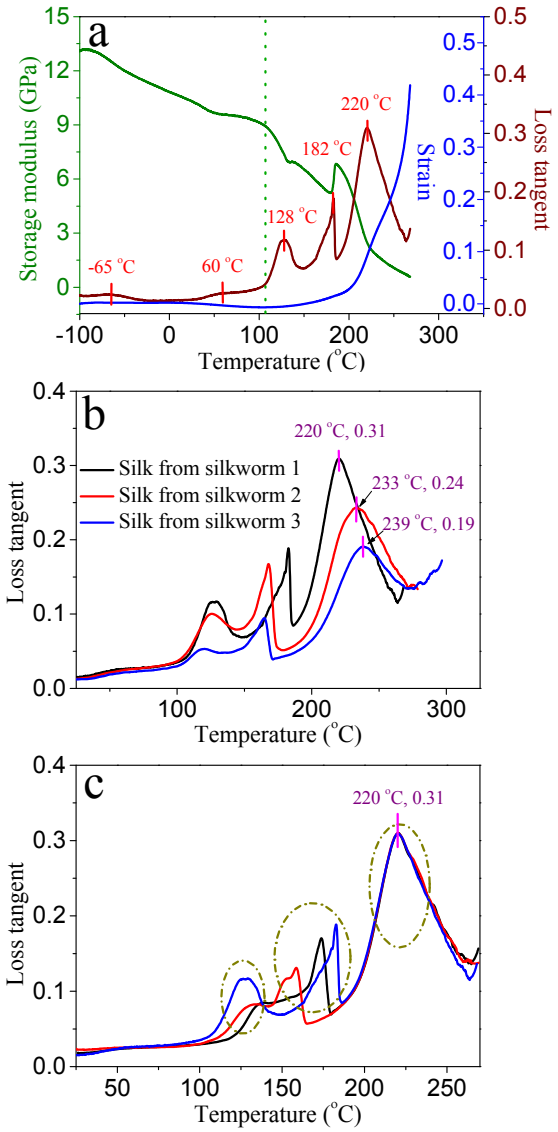

Figure 2. Typical DMTA profile (a) of as-reeled *A. pernyi* silk from silkworm 1, showing the changes in storage modulus, loss tangent, and strain as a function of temperature. Loss tangent profiles of as–reeled *A. pernyi* silks from different silkworms (b) and adjacent silk fibres from silkworm 1 (c). The numbers around the peaks represent the position and height of the corresponding peak. The key loss tangent peaks are highlighted in c.

Large differences also exist in the highest temperature loss peaks of the three different samples and they move to higher temperature and lower peak values (as marked figures near the peaks) in order from silkworm 1, 2 to 3, which means these three samples also possess conspicuously different fractions of disordered structures, since area under the loss peak is proportional to the disordered fraction.[15] Moreover, the strain extension of three samples (Figure

S2b) under the static stress all follows the main T_g peak (Figure 2b) and the sharpest decrease in storage modulus (Figure S2a). The sample from silkworm 1 extends (stretching of the disordered fraction) more than the sample from silkworm 2, and sample from silkworm 3 shows the least extension among the three samples.

To check any possible variability of as-reeled *A. pernyi* silks from the same individual, we also compared the dynamic mechanical properties of adjacent samples from silkworm 1 and the results show that they differ from one another (Figure 2c), which suggests an intrinsic structural variability, although their stress-strain curves are almost coincident (Figure 1a). As in Figure 2b for different silkworms, the two lower temperature loss peaks differ from each other, especially the higher T_g peak which varies between about 155 °C and 185 °C. However, differently, the main T_g peaks at 220 °C are always consistent for samples from the same silkworm. This suggests that the total fraction of disordered structures is consistent for a given silkworm, but that the more disordered or less well bonded structures with lower T_g values can be different. Also, that these more disordered components then transform under combinations of load and temperature during testing to the same consistent higher T_g peak structure, discussed as annealing below.

Figure 3 shows the changes of loss tangent profiles of as-reeled *A. pernyi* silks from different individuals as a function of changes in humidity at a controlled temperature of 80 °C. As the humidity increases, the loss tangents of three samples all increase slowly in the beginning and then more rapidly before a broad loss peak in the humidity range from 67% to 80%, depending on different samples. The loss peaks present here belong to the main glass transitions in silks, and show the similar developing trend for samples from different silkworms as the main T_g peaks in temperature scan (Figure 2b).[43] However, unlike the temperature scan, there are no glass transitions in lower humidity region, which suggests that the more disordered structures may be converted to better bonded structures as the humidity increases through the scans.

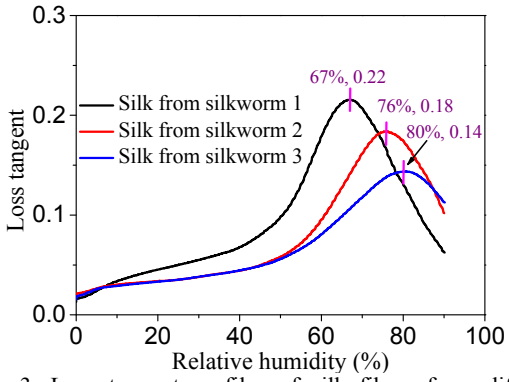

Figure 3. Loss tangent profiles of silk fibres from different silkworms as a function of relative humidity at controlled temperature of 80 °C.

From the previous results, the lower T_g loss peaks are a key source of variability both between silkworms and even within a given silkworm sample set, and that the structures associated with these loss peaks can change to a better bonded structure by virtue of the onset of mobility induced by the transitions. To further shed light on the structural origin of the lower temperature glass transition events, we used cyclical temperature scans to 175 °C to anneal the silks to compare the dynamic mechanical properties before and after annealing process.

Take silk from silkworm 1, for example, Figure 4a shows that the lower temperature loss tangent peaks disappear in the second scan and the corresponding changes in storage modulus associated with these loss peaks are also removed, while the main T_g peak (position and height) in the second scan remains unchanged. This observation indicates that the more disordered structures in the silk fibre can be irreversibly changed to less disordered structures due to the combination of heat and mechanical energy. This is reflected in the stress-strain curves for the same sample in Figure 4b, where the samples show higher elastic modulus and yield stress in the stress-strain curves that follow annealing, which is comparable to the dynamic modulus increases at a reference temperature of 25 °C after annealing treatment (Figure 4a). However, after the yield point, the annealed stress-strain curves exhibit a long plateau, and then tend to follow the same curves as those before annealing. This may suggest that the more ordered structures are just temporarily fixed through annealing and can suddenly revert back to the original structures. Note that annealing treatment of silk fibres from the other two silkworms also generated the same trends as silkworm 1.

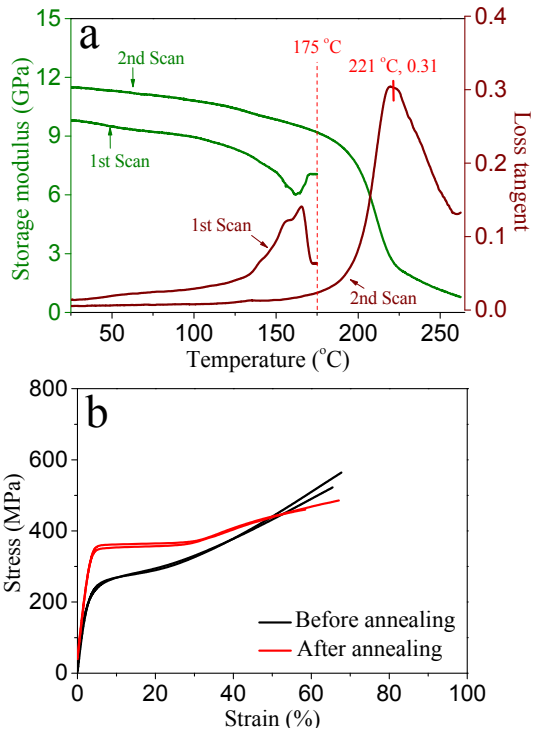

Figure 4. (a) Dynamic mechanical property-temperature profile of 175 °C annealing on silk fibre from silkworm 1; (b) The corresponding stress-strain curves before and after 175 °C annealing, and two separated tests showing the repeatability

In addition, we also investigated the dynamic mechanical properties of the three silk fibres through water annealing (the silk fibre was kept relaxed during annealing), with the results of loss tangent profiles before and after water contraction shown in Figure 5. After water treatment, the lower temperature loss peaks of three samples all become smaller, especially for silks from silkworm 1 and 2, which indicates that part of more disordered structures is transformed into more ordered structures after water annealing. The main T_g peak of the sample from silkworm 1 moves to higher temperature and lower loss peak value after water contraction, while they show slight shifts to lower temperatures for silk fibres from silkworm 2 and 3. This convergence of the three different silkworm structures after water annealing suggests that they might all have a common equilibrium structure, towards which the variable forms induced by different chemical and processing history in the worms can converge.[18]

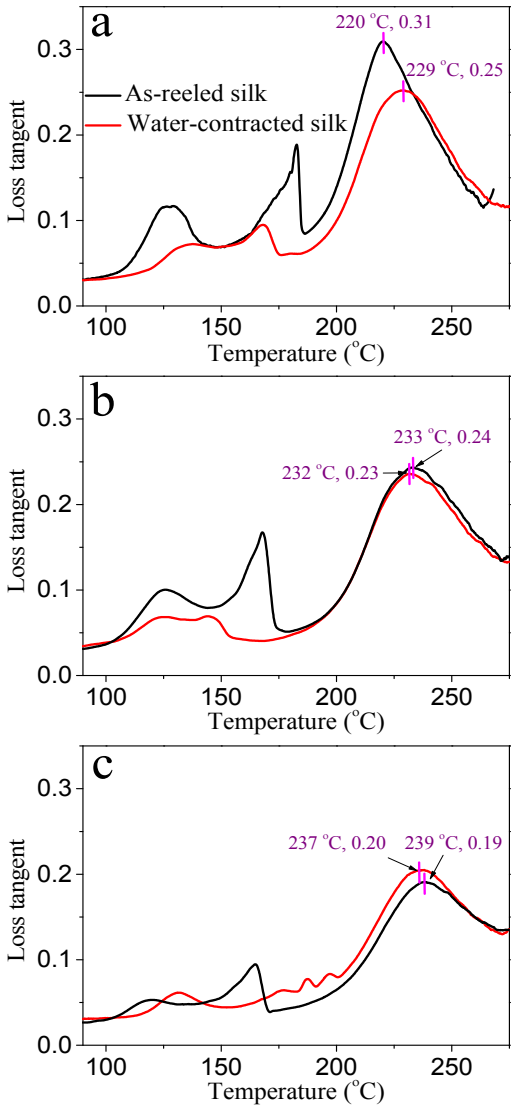

Figure 5. Comparison of loss tangent profiles of silk fibres from different silkworms before and after contraction in water: Silkworm 1 (a), 2 (b), and 3 (c). Same legend for (a), (b) and (c).

Dynamic mechanical properties in different solvents

Combining the techniques from the previous two sections, dynamic mechanical properties of as-reeled *A. pernyi* silks in different solvents were investigated through time scans. As shown in Figure 6a, solvents with different molecular sizes affect the storage modulus to different degrees: ethanol cannot penetrate into all three samples under 50 MPa stress; methanol can gradually enter into the silk fibres with increasing immersion time and reach equilibrium, which gives very different and lower values of storage moduli for different silks than those in air; water as the smallest molecule insinuates itself into all samples immediately after the silk fibres are immersed in it and the three samples show similar storage modulus in water. This convergence of the storage modulus agrees with the trend towards an equilibrium structure discussed for Figure 5 with water annealing.

We also examined the effect of static loading on the penetration of solvents in silks. Using the more disordered silkworm 1 shown in Figure 6b, they initially become more accessible to ethanol with increasing static stress, and this is more significant when the static stress approaches the yield stress (dark green curve in Figure 6b), but these silks become insensitive to ethanol again when static stress is above yield stress (deep teal curve in Figure 6b); this appears to be due to a significant stretching and reordering of the fibres in a softened state under the effect of the ethanol. However, for silk fibres from silkworm 2 and 3, ethanol is always unable to penetrate into them within the range of static stress we applied. Besides, the penetration rates of methanol into all three silks showed a clear trend of increasing as the static stress increases (Figure 6b). Interestingly, the effects of solvents on the dynamic mechanical properties of different silks present here are consistent with those on quasi-static tensile properties displayed in Figure 1.

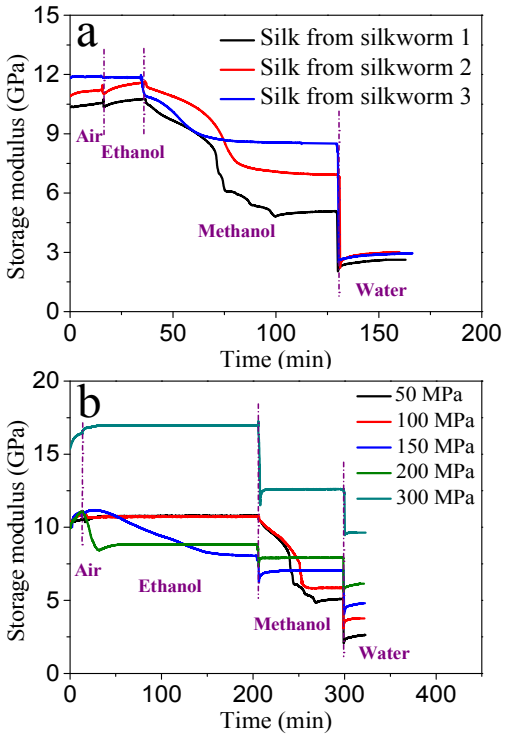

Figure 6. The change of storage modulus in different media through DMTA time scan: (a) as-reeled *A. pernyi* silks from different silkworms under 50MPa static stress and (b) as-reeled *A. pernyi* silks from silkworm 1 under different static stresses.

Structure mechanisms for variability of as-reeled *A. pernyi* silks

These studies confirm previous work that the mechanical properties of a given type of silkworm silk can have a significant variability, even under nominally the same rearing and controlled processing conditions of forced reeling. This applies to both domesticated *B. mori*[45] and wild *A. pernyi*[54] silks. The DMTA observations in this work on *A. pernyi* silk confirm earlier screening work with *B. mori*[42] that these property variations in stress-strain are somehow linked to different structural features, which are identified by a series of discrete loss peaks associated with glass transition events at temperatures around 125, 180, and 220 °C. We have also demonstrated that this variability manifests itself in different responses to a number of different polar solvents, which we previously linked very loosely to the diffusion of the solvents with different molecular sizes through different free volumes available in the more disordered fractions of the silk.[54] This combination of physical spectroscopy and chemical sensitivity present a new and novel way to identify the origin of the variability of properties in chemical structure, and also clarify the structural parameters

required more generally to calculate silk properties. To do this, we identify the parameter of cohesive energy, E_{coh},[55-58] as being common to both solubility and thermo-mechanical properties, and quantitatively demonstrate the self-consistency of our observations using group interaction modelling, GIM, which is presented in detail elsewhere[58, 59] and specifically for silk in previous work[15, 60, 61].

Solubility is determined by the relative solubility parameter, δ, values of the solute and solvent. When the two are equal, the solute will start to dissolve, or at least have a good chemical affinity for the solvent.[55-57] For polar or hydrogen-bonded solids, a general rule is that higher values of solvent δ than solute are good for solubility, because the solvent δ is assumed to be controlled by the polarity (here we ignore details of theory for δ[55-57]). Since we know the solubility parameter values for the solvents, we can deduce the values for silk disordered fractions as they become sensitive to those solvents under different conditions.

Water: 47.9 $MPa^{0.5}$ Methanol: 29.7 $MPa^{0.5}$ Ethanol: 26.2 $MPa^{0.5}$

Solubility parameter, δ(T) ($MPa^{0.5}$) is given at ambient temperature (assume 300 K) in terms of the cohesive energy, $E_{coh}(T)$ (J/mol), and molar volume, V(T) (cc/mol) by

$$\delta(300) = \sqrt{\frac{E_{coh}(300)}{V(300)}} \quad (1)$$

Group contribution values for parameters for the amide group are not specified with reliable values,[56, 57] since the bonding and configuration are determined by the specific local environment, which is highly variable over the range of polymers from which the parameter can be extracted (as also for silk here). A more sophisticated prediction tool is connectivity indices by Bicerano,[62] since the local bonding environment is taken into consideration by specific local structure factors in the structure-property relations. If we take silk to be equivalent to poly(alanine) [15], connectivity indices predicts δ = 31, with specific parameter values of $E_{coh}(300)$ = 52 kJ/mol and V(300) = 54.4 cc/mol. This immediately tells us (for validation purposes) that standard disordered silk is unlikely to be sensitive to methanol or ethanol under normal ambient conditions, but will be sensitive to water. Also, we have now specified two important parameters for GIM modelling, $E_{coh}(300)$ and V(300), which previously had simply to be estimated, and we can now deduce consistent parameter values for mechanical properties. Before going in more detail, we first need to look at the DMTA loss peaks.

The second important property here is T_g, and the general expression for the different T_g values (subscript n) is given in terms of the absolute minimum energy value of E_{coh} by

$$T_{gn} = 0.2246\theta + 0.0513\frac{E_{coh}}{N} \quad (2)$$

where θ is the skeletal mode reference temperature and N is the number of skeletal mode degrees of freedom: for poly(alanine), θ = 400 K from the molecular weight and the value of N = 8 (-$CHCH_3$- = 4 and -CO-NH- = 4). By running GIM simulations of poly(alanine), we can back-calculate the value of E_{coh} that gives the ambient value of $E_{coh}(300)$ = 52 kJ/mol to be 63 kJ/mol. This predicts the intrinsic T_{g3} = 494 K = 221 °C, which is in excellent agreement with the measured value for silk after annealing.

We can now calculate the effective values of E_{coh} for the other two structures that give T_g peaks at T_{g1} = 120 °C = 393 K and T_{g2} = 180 °C = 453 K (Table 2).

This detail in the cohesive binding energy between molecules is now very important to understand the contributions to different silk properties. We can now separate the different contributions to cohesive energy (all units kJ/mol):

Van der Waal's forces without H-bonds:

-CO- = 18 (van Krevelen 17.5) -NH- = 9 -CHCH3- = 9

H-bonds (standard GIM value = 10):

Not-cooperative = 10 cooperative = 14

The different T_g values can now be understood in more physical terms. The lowest T_{g1} = 120 °C is disordered silk with just one hydrogen bond per peptide segment, due to poor packing of the amide units (Table 2). The next T_{g2} = 180 °C is very important, because this is characteristic of reconstituted silk[40] that has been prepared by dissolving in a chaotropic solvent to make the peptide chains very disordered; this means that the hydrogen bonds cannot form cooperative stacking that reinforces the electronic structure (Table 2). Finally, the main T_{g3} = 221 °C is special because the hydrogen bonding is reinforced by cooperative stacking of the bonds in helical-like configurations (Table 2), which has been demonstrated at a fundamental level by *ab initio* QM simulations[63]. This highest T_g is also special because it is the intrinsic T_g of natural silk, formed by the spontaneous denaturation of dope under stress. Notice in Figure 2 that the value of T_{g3} increases slightly from silkworm 1 to silkworm 3, which is consistent with gradually increasing fractions of order in the silk, which increases the bonding polarity and bond strength. This will be important in future modelling to understand the effect of processing conditions, and is a key difference between reconstituted and natural silk.

Table 2 Calculated E_{coh} using Eq 2 and suggested hydrogen bond stacking state

T_g (K)	E_{coh} (kJ/mol)	H-bonds	State
494	63	2	Cooperative
453	57	2	Not cooperative
393	47	1	Not cooperative

We can now make direct connections between solubility parameter effects and glass transitions/yield values. Below, the GIM predicted solubility parameter is plotted as a function of temperature for the three different hydrogen bonded disordered structures (Figure 7), labelled by their T_g values associated with the specific cohesive energy of each structure. The T_g values are also equivalent to the yield points in stress-strain plots.[15, 60] The values of δ at ambient temperature are also marked.

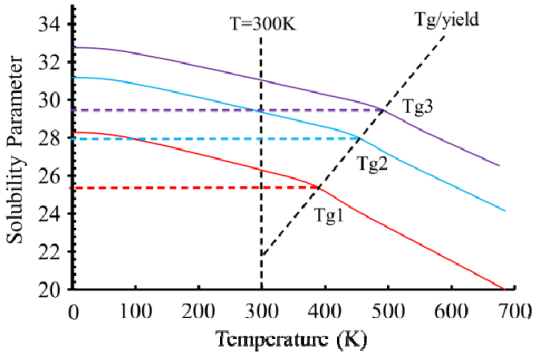

Figure 7. Predicted solubility parameter as a function of temperature for the three different disordered structures. The values of δ at ambient temperature and T_g are marked.

The first point to note is that solvent is unlikely to penetrate the more ordered shell structures of the fibre, due to the crystallinity, unless the sample is stretched under load to create free volume.

Looking at the three values of solubility parameter for the solvents relative to δ (T_g) (Table 3), we see that:

Water (47.9) always has a higher solubility parameter than the disordered fractions, so can always be accepted.

Methanol (29.7) will marginally be accepted for the highest T_g = 494 K at yield (silk 3), but will be accepted for both the lower T_g values at yield (silkworms 1 and 2).

Ethanol (26.2) will not be accepted for the two higher T_g values at yield, but will be accepted by the lowest T_g = 393 K. Since sample from silkworm 1 consistently has high fractions of T_{g1}, ethanol must affect silkworm 1, as shown in Figure 1b. Sample from silkworm 3 has consistently low fractions of T_{g1}, and so is not affected by ethanol at yield (Figure 1c). Silkworm 2 appears to be right on the threshold of effect by ethanol, and larger strains allow great penetration, as shown in Figure 1b.

Table 3 Calculated solubility parameter for the three T_g values using Eq1

Disorder T_g/K (^{o}C)	δ (300)	δ (T_g)
494 (221)	31.0	29.4
453 (180)	29.4	28.0
393 (120)	26.3	25.3

When solvent is absorbed into a structure, the T_g value drops dramatically due to the extra degrees of freedom of the small solvent molecules, and the disordered fraction will behave as a rubberlike material, as discussed in the previous solvent paper[54]. Therefore, higher fractions of the lower T_g disorder will make the silk more sensitive to methanol and then eventually ethanol at yield.

Another important effect to quantify the variability in the silk samples is the overall ordered fraction. This is done semi-quantitatively from the size of the main T_{g3} = 221 °C peak, since the area under the loss tangent peak is proportional to the disordered fraction undergoing the glass transition.[15, 59, 60] However, we needed to run full GIM simulations with the new parameter values to get a best fit between ordered fraction and properties found from the DMTA and stress-strain curves for the three silks. Previously, natural *A. pernyi* silk has been assigned an intrinsic ordered fraction of $f_o = 0.55$.[18] Silk fibre from silkworm 2 has this value, but silkworms 1 and 3 are more and less disordered respectively (Table 4). These calculated values agree well with the relative fractions estimated from the highest T_g loss peak heights, shown in Table 4 as values scaled relative to the lowest value of f_o = 0.40 in silkworm 1. In addition, Figure S3 shows an FTIR analysis of the three silks, and allows a relative value of the ordered fraction to be estimated from the peak height at 965 cm^{-1}, which are again given in Table 4 as values scaled relative to the lowest value of f_o = 0.40 in silkworm 1. Here we assume that the ordered fraction is *β*-sheet fraction.

Table 4 Calculated ordered fraction of the three as-reeled *A. pernyi* silks relative to scaled values of f_o estimated from the relative height of the highest T_g loss peaks and FTIR observations

Samples	f_o (f_{dis})	T_g loss peak	FTIR beta
Silkworm 1	0.40 (0.60)	0.40	0.40
Silkworm 2	0.55 (0.45)	0.54	0.52
Silkworm 3	0.65 (0.35)	0.65	0.61

The GIM model simulations for the three silks with these fractions of order and disorder are given for reference in Supporting Information, together with parameter values discussed for solubility parameter above, and will be reported separately as a more detailed modelling paper, based upon the observations reported here.

We can also see from the insets in Figure 1 that samples from silkworm 1 appears less sheared than samples from silkworm 2, and samples from silkworm 3 is more sheared than those from silkworm 2, from the shapes and relative thickness. This implies that more shear has induced greater order, which also implies that the hydrogen bonding may be more ordered (similar to post-draw[39]). So we can deduce some trends in relative ordering from the solvent effects and mechanical properties:

Silk fibre from silkworm 1 has a significant fraction of the T_{g1} disorder, since it absorbs ethanol;

Silk fibre from silkworm 2 has a smaller fraction of the T_{g1} disorder (small ethanol) but significant T_{g2} (methanol);

Silk fibre from silkworm 3 has very little T_{g1}, and a small fraction of T_{g2}.

Thus, the solvent effects and the glass transitions are now at least self-consistent in their effect on dynamic mechanical properties. We will need to investigate these effects in more detail using the DMTA and stress-strain relations under load to make a quantitative analysis of the fractions of each discrete disordered structure that are present in any silk sample, but the common theme seems to be that more shear during processing generates more order overall, and higher cooperativity of the hydrogen bonding. This is also consistent with structural changes under increasing load presented in Figure 6, where free volume increase up to yield, but then decreases as the higher loads stretch the macromolecules and increase order.

Unfortunately, these analyses do not identify the way that structural variability originates in the silk spinning process, such as higher shear rates due to duct constraints by the silkworm or premature coagulation due to loss of chemical control under stress, but the insights provided by the new model may provide important clues.

Conclusions

Combination of DMTA techniques and polar solvent penetration has been used to investigate the origin of variability in as-reeled *A. pernyi* silks from different individuals. Quasi-static tensile curves of as-reeled *A. pernyi* silks tested in different media suggest considerable variability of tensile properties of silk fibres from different silkworms. The dynamic mechanical properties as a function of temperature or humidity through the glass transition region of different silks demonstrate that different disordered structures with different hydrogen bond stacking states exist in the amorphous regions and they are dramatically different for silks from different individuals. Among them, the more disordered structures linked with the two lower temperature loss peaks can be converted to more ordered structures through high temperature or water annealing. The link between solubility parameter effects of solvents and the three glass transition values has been quantitatively simulated. The overall ordered fractions of the silks from different individuals predicted by GIM modelling agree well with DMTA and FTIR observations. Our results present here shed new light on the structural origin of the variability in as-reeled *A. pernyi* silks and will provide important information for demystifying the variability of other natural proteins and synthetic polymer fibres.

Acknowledgements

For funding, the authors thank the National Natural Science Foundation of China (NSFC 21034003), and Program of Shanghai

Subject Chief Scientist (12XD1401000) for support. The authors also acknowledge the kind help of Dr. Min Chen at Shanghai Synchrotron Radiation Facility for the measurement of S-FTIR microspectroscopy.

Notes and references

[a]State Key Laboratory of Molecular Engineering of Polymers, Laboratory of Advanced Materials and Department of Macromolecular Science, Fudan University, Shanghai 200433, People's Republic of China. E-mail: zzshao@fudan.edu.cn

[b]Department of Zoology, University of Oxford, Oxford, OX1 3PS, UK. E-mail: david.porter@zoo.ox.ac.uk

[c]International Research Centre for Biological and Nature-inspired Materials, Department of Materials Science and Engineering, Beihang University, Beijing 100191, People's Republic of China.

Electronic Supplementary Information (ESI) available: [Fracture end of as-reeled *A. pernyi* silk from silkworm 1 broken in liquid nitrogen, storage modulus and static strain of as-reeled *A. pernyi* silks from different silkworms, S-FTIR method and microspectra as well as Group Interaction Modelling of Silk]. See DOI: 10.1039/b000000x/

1. C. L. Craig, *Ann. Rev. Entomol.*, 1997, **42**, 231-267.
2. J. M. Gosline, P. A. Guerette, C. S. Ortlepp and K. N. Savage, *J. Exp. Biol.*, 1999, **202**, 3295-3303.
3. Z. Z. Shao and F. Vollrath, *Nature*, 2002, **418**, 741-741.
4. X. Y. Liu, N. Du, J. Narayanan, L. A. Li, M. L. M. Lim and D. Q. Li, *Biophys. J.*, 2006, **91**, 4528-4535.
5. C. J. Fu, Z. Z. Shao and F. Vollrath, *Chem. Commun.*, 2009, **43**, 6515-6529.
6. S. Keten, Z. P. Xu, B. Ihle and M. J. Buehler, *Nat. Mater.*, 2010, **9**, 359-367.
7. F. G. Omenetto and D. L. Kaplan, *Science*, 2010, **329**, 528-531.
8. F. Vollrath, D. Porter and C. Holland, *Soft Matter*, 2011, **7**, 9595-9600.
9. F. Vollrath, D. Porter and C. Holland, *MRS. Bull.*, 2013, **38**, 73-80.
10. Y. Termonia, *Macromolecules*, 1994, **27**, 7378-7381.
11. A. H. Simmons, C. A. Michal and L. W. Jelinski, *Science*, 1996, **271**, 84-87.
12. D. T. Grubb and L. W. Jelinski, *Macromolecules*, 1997, **30**, 2860-2867.
13. J. D. van Beek, S. Hess, F. Vollrath and B. H. Meier, *Proc. Natl. Acad. Sci. U. S. A.*, 2002, **99**, 10266-10271.
14. Y. Liu, Z. Z. Shao and F. Vollrath, *Nat. Mater.*, 2005, **4**, 901-905.
15. D. Porter, F. Vollrath and Z. Shao, *Eur. Phys. J. E*, 2005, **16**, 199-206.
16. T. Ackbarow, X. Chen, S. Keten and M. J. Buehler, *Proc. Natl. Acad. Sci. U. S. A.*, 2007, **104**, 16410-16415.
17. F. Grater, M. Cetinkaya, S. B. Xiao, B. Markert and W. Stacklies, *Biophys. J.*, 2011, **100**, 1298-1305.
18. C. J. Fu, D. Porter, X. Chen, F. Vollrath and Z. Z. Shao, *Adv. Funct. Mater.*, 2011, **21**, 729-737.
19. G. R. Plaza, J. Pérez-Rigueiro, C. Riekel, G. Belén Perea, F. Agulló-Rueda, M. Burghammer, G. V. Guineaad and M. Elicesad, *Soft Matter*, 2012, **8**, 6015– 6026.
20. F. Paquet-Mercier, T. Lefèvre; M. Auger and M. Pézolet, *Soft Matter*, 2013, **9**, 208-215.
21. D. Porter, J. Guan and F. Vollrath, *Adv. Mater.*, 2013, **25**, 1275-1279.
22. D. L. Dunaway, B. L. Thiel and C. Viney, *J. Appl. Polym. Sci.*, 1995, **58**, 675-683.
23. J. Perez-Rigueiro, C. Viney, J. Llorca and M. Elices, *J. Appl. Polym. Sci.*, 1998, **70**, 2439-2447.
24. B. Madsen, Z. Z. Shao and F. Vollrath, *Int. J. Biol. Macromol.*, 1999, **24**, 301-306.
25. J. Perez-Riguero, M. Elices, J. Llorca and C. Viney, *J. Appl. Polym. Sci.*, 2001, **82**, 2245-2251.
26. M. A. Garrido, M. Elices, C. Viney and J. Perez-Rigueiro, *Polymer*, 2002, **43**, 4495-4502.
27. T. A. Blackledge, R. A. Cardullo and C. Y. Hayashi, *Invertebr. Biol.*, 2005, **124**, 165-173.
28. H. P. Zhao, X. Q. Feng and H. J. Shi, *Mat. Sci. Eng. C*, 2007, **27**, 675-683.
29. F. Vollrath and D. Porter, *Soft Matter*, 2006, **2**, 377-385.
30. B. Mortimer, C. Holland and F. Vollrath, *Biomacromolecules*, 2013, **14**, 3653–3659.
31. P. Colomban, H. M. Dinh, A. Bunsell and B. Mauchamp, *J. Raman Spectrosc.*, 2012, **43**, 425-432.
32. P. Colomban and H. M. Dinh, *J. Raman Spectrosc.*, 2012, **43**, 1035-1041.
33. P. Colomban, H. M. Dinh, A. Tournie and V. Jauzein, *J. Raman Spectrosc.*, 2012, **43**, 1042-1048.
34. N. G. McCrum, B. E. Read and G. Williams, *Anelastic and Dielectric Effects in Polymeric Solids*, John Wiley & Sons, London, 1967.
35. D. L. Kaplan, W. W. Adams, B. Farmer and C. Viney, *ACS Symp. Ser.*, 1994, **544**, 2-16.
36. M. Tsukada, G. Freddi, N. Kasai and P. Monti, *J. Polym. Sci. Pol. Phys.*, 1998, **36**, 2717-2724.
37. Y. Yang, X. Chen, Z. Z. Shao, P. Zhou, D. Porter, D. P. Knight and F. Vollrath, *Adv. Mater.*, 2005, **17**, 84-88.
38. T. A. Blackledge, J. E. Swindeman and C. Y. Hayashi, *J. Exp. Biol.*, 2005, **208**, 1937-1949.
39. J. W. Yin, E. Q. Chen, D. Porter and Z. Z. Shao, *Biomacromolecules*, 2010, **11**, 2890-2895.
40. Q. Q. Yuan, J. R. Yao, L. Huang, X. Chen and Z. Z. Shao, *Polymer*, 2010, **51**, 6278-6283.
41. R. Anumolu, J. A. Gustafson, J. J. Magda, J. Cappello, H. Ghandehari and L. F. Pease, *Acs Nano*, 2011, **5**, 5374-5382.
42. J. Guan, D. Porter and F. Vollrath, *Biomacromolecules*, 2013, **14**, 930-937.
43. J. Guan, F. Vollrath and D. Porter, *Biomacromolecules*, 2011, **12**, 4030-4035.
44. J. Guan, D. Porter and F. Vollrath, *Polymer*, 2012, **53**, 2717-2726.
45. B. Mortimer *et al*, *Submitted to Acta Biomaterialia*.
46. P. A. Guerette, D. G. Ginzinger, B. H. F. Weber and J. M. Gosline, *Science*, 1996, **272**, 112-115.
47. H. Sezutsu and K. Yukuhiro, *J. Mol. Evol.*, 2000, **51**, 329-338.
48. M. Tsukada, G. Freddi, Y. Gotoh and N. Kasai, *J. Polym. Sci. Pol. Phys.*, 1994, **32**, 1407-1412.
49. Y. Nakazawa and T. Asakura, *Macromolecules*, 2002, **35**, 2393-2400.
50. M. Tsukada, G. Freddi, P. Monti, A. Bertoluzza and N. Kasai, *J. Polym. Sci. Pol. Phys.*, 1995, **33**, 1995-2001.
51. G. Freddi, P. Monti, M. Nagura, Y. Gotoh and M. Tsukada, *J. Polym. Sci. Pol. Phys.*, 1997, **35**, 841-847.
52. M. Z. Li, W. Tao, S. Kuga and Y. Nishiyama, *Polym. Advan. Technol.*, 2003, **14**, 694-698.
53. S. J. Ling, Z. M. Qi, D. P. Knight, Y. F. Huang , L. Huang, H. Zhou, Z. Z.

Shao, and X. Chen *Biomacromolecules*, 2013, **14**, 1885–1892.
54. Y. Wang, D. Porter and Z. Z. Shao, *Biomacromolecules*, 2013, **14**, 3936-3942.
55. A. F. M. Barton, *Chem. Rev.*, 1975, **75**, 731-753.
56. A. F. M. Barton, *Handbook of Solubility Parameters and Other Cohesion Parameters*, CRC Press, Florida, 1983.
57. D. W. van Krevelen, *Properties of Polymers, Third Edition*, Elsevier, Amsterdam, 1993.
58. D. Porter, *Group Interaction Modelling of Polymer Properties*, Marcel Dekker, New York, 1995.
59. D. Porter and P. J. Gould, *Int. J. Solids Struct.*, 2009, 46, 1981-1993.
60. F. Vollrath and D. Porter, *Appl. Phys. A*, 2006, **82**, 205-212.
61. C. J. Fu, D. Porter and Z. Z. Shao, *Macromolecules*, 2009, **42**, 7877-7880.
62. J. Bicerano, *Prediction of Polymer Properties*, Marcel Dekker, New York, 1993.
63. J. Ireta, J. Neugebauer, M. Scheffler, A. Rojo and M. Galvan, *J. Phys. Chem. B*, 2003, **107**, 1432-1437.

